01 Nov 2000

# Binary Condensation in a Supersonic Nozzle

Barbara Ellen Wyslouzil

Christopher H. Heath

Janice L. Cheung

Gerald Wilemski
*Missouri University of Science and Technology*, wilemski@mst.edu



## Recommended Citation

B. E. Wyslouzil et al., "Binary Condensation in a Supersonic Nozzle," *Journal of Chemical Physics*, vol. 113, no. 17, pp. 7317-7329, American Institute of Physics (AIP), Nov 2000.
The definitive version is available at https://doi.org/10.1063/1.1312274

# Binary condensation in a supersonic nozzle

Barbara E. Wyslouzil,[a] Christopher H. Heath, and Janice L. Cheung
*Department of Chemical Engineering, Worcester Polytechnic Institute, Worcester, Massachusetts 01609-2280*

Gerald Wilemski
*Department of Physics and Cloud and Aerosol Sciences Laboratory, University of Missouri-Rolla, Rolla, Missouri 65409-0640*

(Received 8 June 2000; accepted 3 August 2000)

We present data from the first systematic studies of binary condensation in supersonic nozzles. The apparatus used to conduct the experiments is described in detail, and the important issues of stability and reproducibility of the experiments are discussed. Experiments were conducted with water, ethanol, propanol, and binary mixtures of these compounds. Onset was determined in the temperature range of 190–215 K, and for each mixture composition the pressures of the condensible species at an onset temperature of 207 K were determined. For the ideal ethanol–propanol mixtures, the onset pressures at constant temperature vary almost linearly between those of the pure components. In contrast the isothermal onset pressures for the nonideal water–ethanol and water–propanol mixtures lie below the straight line joining the pure component values. This large reduction in the total pressure of condensible at onset for the aqueous alcohol mixtures is indicative of a strong mutual enhancement in the particle formation process. © *2000 American Institute of Physics.* [S0021-9606(00)51441-X]

## I. INTRODUCTION

Predicting the rate at which embryos of a new phase form from a metastable mother phase remains both a fundamental and practical challenge, especially in the presence of multiple condensible species. Experimental apparatuses have been developed to measure nucleation rates in unary and multicomponent systems over a wide range of supersaturations and temperatures.[1] Current techniques include diffusion cloud chambers,[2–4] diffusion flow tubes,[5,6] expansion cloud chambers,[7,8] shock tubes,[9] piston expansion tubes,[10] pulse expansion wave tubes,[11,12] and the fast mixing apparatus.[13,14] Each experimental setup is usually limited to measuring rates over 3–4 orders of magnitude, and no single device can make measurements on all substances of interest. Thus data from a wide range of techniques are required to enhance our understanding of this complex phenomenon.

Unlike other techniques, supersonic nozzles do not yet yield nucleation rates directly because the length of time over which nucleation contributes significantly to particle formation is not easy to determine or control, and accurate determination of the number concentration of particles has only recently become possible.[15,16] Nonetheless, experiments in nozzles are extremely important because they provide higher rates of cooling, higher supersaturations, and much higher nucleation rates than all of the techniques mentioned above. Moreover, in nozzle experiments, the critical clusters are predicted to be very small, containing on the order of 5–10 molecules, and thus the nucleation kinetics is sensitive to the formation of the smallest molecular clusters. Furthermore, assumptions that may be valid for larger clusters, for example the compact spherical shape, are clearly invalid for these tiny clusters.[17] A more practical concern is that nozzle operating conditions, with cooling rates of $\sim 1$ K/$\mu$s, are more typical of important industrial applications such as aerodynamic and turbomechanical flows for which homogeneous nucleation can have serious consequences.[18]

The fluid mechanics of nozzles is well defined and understood,[18,19] and under steady flow conditions the entire history of the expansion is easily obtained by measuring one of the state variables as a function of position. Static pressure and density are the usual candidates.[20–22] Because the phase transition releases heat into the flow, the onset of condensation is detected as a deviation of a condensing flow property from its isentropic value. Alternatively, a sharp increase in the light scattering signal has been used to detect the presence of particles, especially in cases where state variable measurements are difficult.[23] Recently, small angle neutron scattering (SANS) experiments[15,16] have provided additional independent information about the size distribution of the aerosol formed in the nozzle that is unobtainable from earlier light scattering studies.[22] The data from SANS experiments and state variable measurements together place severe constraints on acceptable models of nucleation and droplet growth under these highly supersaturated conditions. An analysis with preliminary conclusions for the condensation of $H_2O$ and $D_2O$ is available.[24,25]

Binary nucleation experiments were first conducted by Flood[26] using an expansion cloud chamber to study the onset of condensation in the ethanol–water system. Since this pioneering work, binary nucleation has been studied using many of the techniques listed above. Initially only the conditions at the onset of condensation were reported,[27–29] but now iso-

[a]Author to whom correspondence should be addressed; electronic mail: barbaraw@wpi.edu

 

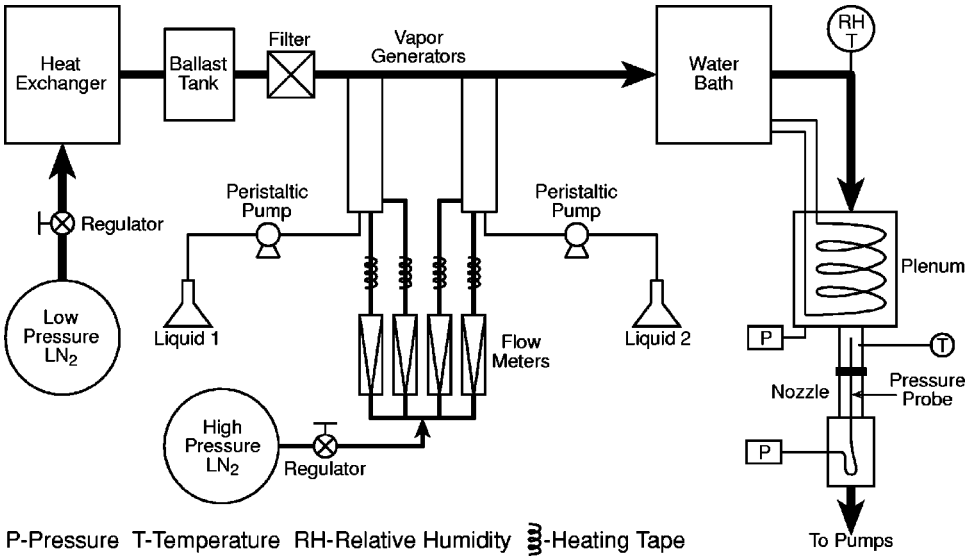


FIG. 1. A schematic diagram of the experimental apparatus.

thermal binary nucleation rates have been measured for a large number of systems that form both ideal[30] and nonideal liquid mixtures.[10,31–34] Until recently, only preliminary experimental results for the onset of binary condensation in supersonic nozzles have been reported.[35,36] For many of these experiments the goal was to identify when low levels of impurities affected the results of unary condensation experiments.[36] In addition to the data presented here, we have also completed a systematic study of binary condensation of $D_2O$–$H_2O$ in the supersonic nozzle.[24,25]

One of the most interesting results of isothermal nucleation rate experiments has been the strong mutual enhancement observed for the binary nucleation of water–*n*-alcohol droplets.[10,31–33] Even though the pressure of water–*n*-alcohol mixtures deviates positively from that of an ideal solution, the activities of the individual components required to maintain a constant nucleation rate are significantly lower than those expected for an ideal solution. The enhancement persists even when the two species exhibit a miscibility gap for bulk mixtures. The experimental trend is consistent with the idea that surface enrichment by the species with the lower surface tension (alcohol) greatly reduces the surface free energy of the critical clusters, thus lowering the barrier to nucleation. In expansion cloud chamber experiments, where critical clusters contain between 20 and 100 molecules, the molecular content of the critical clusters has been measured directly[30,32–34] by applying the nucleation theorem[30,32,37] to the isothermal nucleation rate data. For a sequence of experiments using water and ethanol,[32] the molecular content of the critical clusters was consistent with a model that incorporated the concept of surface enrichment.[38]

One of the goals of the current work is to see whether the strong enhancement observed at lower supersaturations is also found for conditions yielding critical clusters so small (5–10 molecules) that the distinction between surface and bulk molecules is essentially meaningless. We start by looking at condensation of the three pairs that can be formed by water, ethanol, and propanol. Of these systems, ethanol–water and propanol–water are both nonideal systems and should be strongly influenced by the nonuniform cluster structure that evolves into surface enrichment for larger droplets. In contrast, the behavior of ethanol–propanol should be close to the ideal behavior Strey and Viisanen observed for ethanol–hexanol.[30]

The organization of the paper is as follows. Section II presents a detailed description of the experimental apparatus. The experimental procedures, data reduction, and the reproducibility of the nozzle experiments are addressed in Sec. III. We present our results in Sec. IV and summarize the work and our conclusions in Sec. V. We do not compare the data to theoretical predictions in this paper because onset data are insufficient to uniquely determine the nucleation rate, and our current model for condensation in supersonic expansions does not yet include a binary droplet growth model.

## II. EXPERIMENTAL EQUIPMENT

A schematic diagram of the experimental setup used to conduct the binary condensation experiments is illustrated in Fig. 1. The key components of the apparatus, described in detail below, include: (1) the carrier gas generator, (2) the condensible vapor generators, and (3) the supersonic nozzle and pressure probe.

### A. Carrier gas generation and flow through the system

For convenience and economy, the carrier gas used in the experiments is $N_2$. To generate the $\sim 8.6$ g/s $N_2$ required by the experiments, liquid $N_2$ (LN2) is fed from a 230 L low pressure (100–300 kPa) Dewar into a commercial finned heat exchanger (Thermax Inc, Model TF068) where it evaporates. The total area available for heat transfer is $\sim 17$ m$^2$ and room air is the heat source. The flow rate of the LN2 is controlled using a cryogenic liquid pressure regulator (AW Cash Valve, B12300). The LN2 Dewar is on a balance (Cardinal Scale Inc., RW1000), and the weight of the low pressure LN2 is monitored during an experiment. The carrier gas exits the heat exchanger at about 150 kPa and just slightly below room temperature. Because the onset of condensation is detected by the deviation of the pressure of the condensing

flow curve from that of the corresponding isentropic expansion, precise control of $p_0$ is critical to our ability to observe onset consistently especially when very little heat is added to the flow.

After exiting the heat exchanger, the $N_2$(g) flows through a 0.1 $m^3$ ballast tank and a high volume filter to damp out small pressure oscillations. The cool $N_2$(g) stream mixes with the hot condensible-rich streams from the vapor generators, and the temperature of the combined flow is adjusted by passing it through a copper cooling coil placed in a waterbath (VWR Scientific, Model 1157). After the preliminary temperature adjustment, the relative humidity (RH) of the gas stream is measured using an RH probe (Vaisala Inc., HMP-233). The capacitance of the probe changes with the gas phase activity of $H_2O$ and, to a lesser extent, the gas phase activity of the alcohols. For this reason, the RH probe is only used as an indicator for the presence and stability of the condensible vapor flow. Actual gas phase compositions are calculated from the carrier gas and liquid mass flow rates.

The flow then enters the plenum, a 0.33 m long ISO 200 stainless steel nipple, that contains additional finned copper cooling coils. The fluid circulating through the coils comes from the water bath described earlier. The final temperature adjustment occurs in the plenum and the stagnation pressure of the gas is measured using a high accuracy capacitance manometer (MKS Baratron 690A). The gas velocity in the plenum is ~0.3 m/s, and the gas is effectively at rest compared to the speed of sound in $N_2$ (340 m/s at STP). At the exit of the plenum the gas passes through a 64 mm long flow straightener whose internal dimensions (25.4 mm×12.7 mm) approach those of the nozzle entrance. A high accuracy RTD (Omega Engineering, Type A sensing element) housed in a 1.6 mm stainless steel sheath and located in the center of the flow stream measures the stagnation temperature of the gas $T_0$.

After the flow straightener, the gas flows through the nozzle, the box housing the pressure probe drive, and finally through 75 mm tubing to the two rotary vane vacuum pumps (Busch models RC0160 and RC0250) that provide up to 0.13 $m^3$/s pumping capacity.

### B. Condensible vapor generation

In the vapor generator, a fine mist of the liquid to be vaporized is produced using a simple spray nozzle. Liquid is pumped into this vaporizer using a peristaltic pump (Masterflex Pump Model 7523-20), and the mass flow rate of the material is measured by recording the weight of liquid dispensed during the course of an experiment. Two hot $N_2$(g) streams also enter the vaporizer. The first one warms and breaks the liquid into a fine mist, while the second one provides a flow of sheath air to carry the droplets up the riser tube as they evaporate. Energy is added to both gas streams using heating tapes, and the total energy input is 3–5 times the heat of vaporization of the liquid. To avoid condensation on the walls, the temperature and the flow rates of the liquid and the carrier gas through the vapor generator are such that the final vapor mixture has a gas phase activity $<0.8$.

The gas flows to the vapor generator are controlled by rotameters with the valves located at the outlet, and the pressure at the inlet of the rotameters is maintained at about 400 kPa. Because the combined flow through a single vapor generator is approximately ~2.8 g/s, the $N_2$(g) is taken from the gas line of a high pressure (1–1.5 MPa) LN2 Dewar rather than from a high pressure gas bottle. The rotameters were calibrated by flowing gas at a fixed inlet pressure and weighing the amount of $N_2$ consumed. At the outlet of the riser tube, the hot vapor rich stream mixes with the room temperature carrier gas to form the final, subsaturated gas stream.

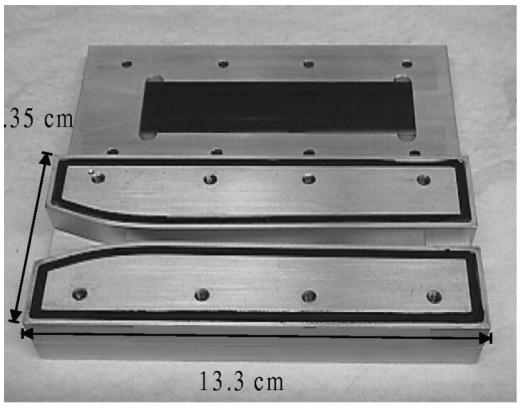


FIG. 2. The Laval nozzle used in the experiments. The key dimensions are given. The flow is from left to right.

For unary nucleation experiments or for binary experiments with fully miscible liquids, only a single vapor generator is required. To investigate binary droplet formation when the two liquids are only partially miscible, a separate generator is used for each liquid. Although all of the mixtures used during these experiments were fully miscible, the dual generator setup was tested by acquiring some of the onset data for the 80 mol % $H_2O$–propanol experiments using separate vapor generators for the $H_2O$ and propanol.

### C. Nozzle and pressure probe

As illustrated in the photograph in Fig. 2, we use a Laval nozzle machined from aluminum with straight side walls and top and bottom blocks that converge and diverge symmetrically at constant angles. The straight converging and diverging sections are joined near the throat by a cubic spline such that in the supersonic region the curved section joins the linear section smoothly; i.e., the composite curve is continuous through the second derivative. This degree of smoothness ensures that there are no weak shocks in the flow downstream of the throat.[39] Because the nozzle is also used to conduct SANS experiments, the side blocks have 95 mm×25 mm×1 mm thick unpolished silicon windows that are transparent to neutrons. To seal the assembly without breaking the windows we use 3.2 mm thick gaskets cut from supersoft neoprene and constrained in shallow o-ring grooves. The nozzle used in these experiments had a converging section 38 mm long, a diverging section 95 mm long, and the upper and lower walls diverge at an angle of 1.8° in the linear region. As designed, the throat is 12.7 mm wide and 5 mm high, the ratio of the area at the exit of the nozzle to the area of the throat $A/A^*$ is 1.58, and the maxi-

mum Mach number $M$ is 1.95 for a gas with $\gamma=1.4$. Here $\gamma$ is the usual ratio of the constant pressure and constant volume heat capacities.

The pressure is measured along the length of the nozzle using a movable probe. The static pressure probe is a 305 mm long 1.6 mm o.d. stainless steel tube with four equally spaced 0.5 mm holes drilled 140 mm downstream from the tip. The offset of the static pressure holes from the tip of the probe is more than twice the minimum distance to avoid affecting the pressure measurements by flow disturbances from the tip.[19] The probe is attached to a linear translation stage that is housed in a separate vacuum-tight box downstream of the nozzle. The central rail of the translation stage is rotated by turning a shaft on the outside of the box. Attached to the shaft are an optical counter and accumulator that track the position of the pressure probe. With this arrangement we can resolve the position of the probe to better than 0.1 mm. The probe is sealed at the upstream tip and is connected to a pressure transducer (MKS Baratron 690A) at the downstream end via a length of Tygon tubing and a vacuum-tight fitting that goes through the side of the probe box. To ensure that the probe travels down the centerline of the nozzle, the probe passes through a hole in a small teflon block attached to the roof of the probe box near the exit of the nozzle. The upstream end of the probe is secured by a piece of coarse mesh with some finer weaving in the central squares at the entrance to the nozzle. The placement of the static pressure holes ensures that the probe is still held at the upstream end by the mesh even when it is in the furthest downstream position.

## III. EXPERIMENTAL PROCEDURES

### A. Determining the gas composition

In theory, the composition of the gas mixture can be directly determined from the mass flow rate measurements, i.e.,

$$y=\frac{\dot{m}_v/\mu_v}{\dot{m}_i/\mu_i+\dot{m}_v/\mu_v}, \tag{1}$$

where $y$ is the mole fraction of condensible vapor in the stream, $\dot{m}$ is a mass flow rate, and $\mu$ is a molecular weight. The subscripts $v$ and $i$ refer to the condensible vapor and the inert carrier gas (here, $N_2$), respectively. Prior to condensation, the pressure of the condensible vapor in the gas stream $p_v$ is given by

$$p_v=yp, \tag{2}$$

assuming ideal gas behavior. In the plenum we denote the partial pressure of the condensible as $p_{v0}$. Straightforward application of Eq. (1), however, introduces unnecessary uncertainty into $y$ because the flow of $N_2$(g) enters the system through two different streams: the main flow and the flow through the vapor generators. Formally propagating the error associated with individual measurements, especially that of the rotameters, seriously overestimates the uncertainty in $y$ and $p_v$.

A better estimate for $y$ comes from assuming that the molar flow rate through the nozzle is fixed by the stagnation conditions in the plenum, $p_0$ and $T_0$, and by the nozzle throat area $A^*$, and thus $y$ is given to lowest order by

$$y^0=\frac{\dot{m}_v/\mu_v}{\dot{m}_i^0/\mu_i}. \tag{3}$$

Here, $\dot{m}_i^0/\mu_i$ is the molar flow rate of pure $N_2$(g) through the nozzle at $p_0$ and $T_0$. The value of $\dot{m}_i^0/\mu_i$ can be determined to better than 0.1% by measuring the flow of $N_2$(g) through the nozzle at constant $(p_0,T_0)$ for about 1 h. The uncertainty in $y^0$ is then determined mainly by the measurement error in $\dot{m}_v$, which is at most 1%. As demonstrated in the Appendix, an improved estimate for $y$ can be found by subjecting Eq. (1) to a first order Taylor expansion. The result is

$$y=y^0/(1-y^0d), \tag{4}$$

where $y^0$ is given by Eq. (3) and $d$ is an easily calculated parameter defined in the Appendix. The value of $d$ depends on the composition of the condensible vapor and equals 0.126 for pure water, 0.783 for pure ethanol, and 1.31 for pure *n*-propanol. For mixtures, the values of $d$ obviously lie between the appropriate pair of pure component values. The largest value for $y^0d$ in these experiments was 0.002, and thus the error introduced by using Eq. (3) rather than Eq. (4) was less than 0.2%.

### B. Measuring and interpreting pressure profiles

After the system reaches stable operating conditions, a pressure trace $p(x)$ is measured starting with the pressure probe at the farthest upstream position, 2–3 cm before the throat. Several pressure measurements are made in the subsonic region; in the vicinity of the throat the measurements are made at 0.1 mm intervals, and downstream of the throat the pressure is measured at 1.0 mm intervals to the end of the nozzle. In addition to recording the static pressure at each location $x$, the values of $T_0$, $p_0$, RH, the weight of the low pressure $LN_2$ Dewar, and the time are recorded using a digital-to-analog board (Keithly DAS1602) and a desk-top computer. Usually a burst of 21 measurements are taken for each variable in less than 1 s via direct memory access mode, and the average value of each variable and its corresponding standard deviation are computed. In addition, the mass flow rate of liquid entering the system is recorded manually for the time period of the static measurements.

Because of the boundary layers that develop along the walls and some play in the nozzle assembly, the effective area ratio of the nozzle differs from that of the design. The effective shape of the nozzle at the desired values of $p_0$ and $T_0$ is derived from the dry pressure trace data using the relationships for isentropic expansions

$$M^2=\frac{2}{\gamma-1}\left[\left(\frac{p}{p_0}\right)^{(1-\gamma)/\gamma}-1\right], \tag{5}$$

and

$$\frac{A}{A^*}=\frac{1}{M}\left[\frac{2+(\gamma-1)M^2}{\gamma+1}\right]^{(\gamma+1)/(2\gamma-2)}. \tag{6}$$

Here $M=u/a$ is the Mach number, $u$ is the local velocity, $a=\sqrt{\gamma RT/\mu_i}$ is the local speed of sound, $\gamma$ is the ratio of

constant pressure and constant volume heat capacities, and $R$ is the universal gas constant. After measuring the dry pressure trace, the experiments are repeated using the desired gas mixtures.

To determine the conditions at onset we need to compare the properties of the condensing flow to the expansions that would have occurred in the absence of condensation. The first step is to locate the position of the throat for each set of pressure trace data. For a given gas mixture, the value of $p/p_0$ at the throat is given by

$$\frac{p}{p_0}=\left[\frac{1+\gamma_m}{2}\right]^{\gamma_m/(1-\gamma_m)}. \tag{7}$$

Here, for a thermally perfect gas,

$$\gamma_m=C_{\mathrm{pm}}/(C_{\mathrm{pm}}-R), \tag{8}$$

where $\gamma_m$ is the ratio of heat capacities for the mixture and $C_{\mathrm{pm}}$ is the molar heat capacity at constant pressure of the mixture

$$C_{\mathrm{pm}}=\sum_j y_j C_{pj}. \tag{9}$$

The mole fraction and the constant pressure heat capacity of component $j$ in the mixture are $y_j$ and $C_{pj}$, respectively. When the amount of condensible material in the stream is small, the condensing flow curve follows the dry pressure trace very closely in the region prior to onset. At higher condensible mass fractions there is a slight but noticeable offset due to the difference between $\gamma$ and $\gamma_m$. To account for this difference, we use the area ratios based on the dry pressure trace to calculate the properties (pressure, temperature, density, and velocity) of an isentropically expanding gas using Eqs. (5) and (6) with $\gamma=\gamma_m$. We call this useful but fictitious flow curve the ''mixture isentrope.''

The key unmeasured properties of the condensing flow are the local gas velocity $u$, the temperature $T$, the density $\rho$, and the condensate mass fraction $g$. To derive these properties from the dry and condensing flow pressure traces, we integrate the diabatic flow equations cast in a form with pressure and area ratio as the known quantities.[18] The first two equations are the mass balance equation

$$u=\frac{u^*\rho^*A^*}{\rho A}, \tag{10}$$

and the density change equation,

$$d\left(\frac{\rho}{\rho_0}\right)=\left[\frac{1}{\gamma_m}\left(\frac{u^*}{u}\right)^2\frac{T_0}{T^*}\right]d\left(\frac{p}{p_0}\right)-\left(\frac{\rho}{\rho_0}\right)d\ln\left(\frac{A}{A^*}\right), \tag{11}$$

where the starred quantities and $\gamma_m$ are evaluated for the conditions at the throat. Equation (11) is a combination of the momentum equation, $\rho u\,du=-dp$, and the mass balance equation, Eq. (10).

The remaining two diabatic flow equations differ from the simpler, but incorrect, equations given elsewhere.[18] As condensible vapor is removed from the gas stream by condensation, the ideal gas mixture equation of state must reflect the changing composition of the gas stream. Earlier presentations[18] neglected this effect, but the correct equations can easily be derived from the basic formalism developed previously to invert gas dynamic density measurements.[20]

In explicit form, the complete temperature change equation takes the form

$$d\left(\frac{T}{T_0}\right)=\left[w_0(g)-\frac{1}{\gamma_m}\left(\frac{u^*}{u}\right)^2\frac{T}{T^*}\right]\frac{\rho_0}{\rho}d\left(\frac{p}{p_0}\right)+\left(\frac{T}{T_0}\right)\times\left[d\ln\left(\frac{A}{A^*}\right)+w(g)dg\right]. \tag{12}$$

Here, the quantities $w_0(g)$ and $w(g)$ are defined as

$$w_0(g)=\mu/[\mu_0(1-g)], \tag{13}$$

and

$$w(g)=\mu/[\mu_v(1-g)], \tag{14}$$

where $\mu$ is the mean molecular weight of the *gas* mixture when the condensate mass fraction $g$ is nonzero and $\mu_0$ is the corresponding value of $\mu$ at the stagnation conditions when $g=0$. Equation (12) is a combination of the energy equation, the modified equation of state,[20] and Eq. (11).

When the total amount of condensible is small enough, or when very little material has condensed, the temperature equation may be simplified to the following form:[18]

$$d\left(\frac{T}{T_0}\right)=\left[1-\frac{1}{\gamma_m}\left(\frac{u^*}{u}\right)^2\frac{T}{T^*}\right]\frac{\rho_0}{\rho}d\left(\frac{p}{p_0}\right)+\left(\frac{T}{T_0}\right)d\ln\left(\frac{A}{A^*}\right). \tag{15}$$

For more general applicability and higher accuracy, it is necessary to determine how $g$ varies in the nozzle in order to integrate Eq. (12). This may be done by first combining the energy equation for the heat added per unit mass of gas flow $q$, with Eq. (12) to eliminate $dT$, followed by use of the definition of $dq$ in terms of $g$

$$dq=L(T)dg, \tag{16}$$

where $L(T)$ is the latent heat per unit mass of condensate. The result is

$$\left[\frac{L(T)}{c_PT_0}-\frac{T}{T_0}w(g)\right]dg=\frac{\rho_0}{\rho}\left[h-\frac{1}{\gamma_m}\left(\frac{u^*}{u}\right)^2\frac{T}{T^*}\right]d\left(\frac{p}{p_0}\right)+\left(\frac{T}{T_0}\right)d\ln\left(\frac{A}{A^*}\right), \tag{17}$$

where

$$h=w_0(g)-\frac{c_{p0}}{c_p}\left(\frac{\gamma_0-1}{\gamma_0}\right), \tag{18}$$

$c_p$ is the specific heat of the flowing gas stream ($c_p=C_{\mathrm{pm}}/\mu$) and $c_{p0}$ and $\gamma_0$ are the values of $c_p$ and $\gamma_m$, respectively, at stagnation conditions. As for Eq. (15), when $g$ is small and no condensation has occurred at the throat, $h=1/\gamma_m$, and the right hand side of Eq. (17) simplifies to the form given elsewhere.[18] Note that because the term $c_pTw(g)$ ($\approx L(T)/3$) generally cannot be neglected in comparison to $L(T)$, the left hand side can never be simplified to the form given by Wegener[18] without incurring an error in the value of $g$ that is found. Because very little material has condensed

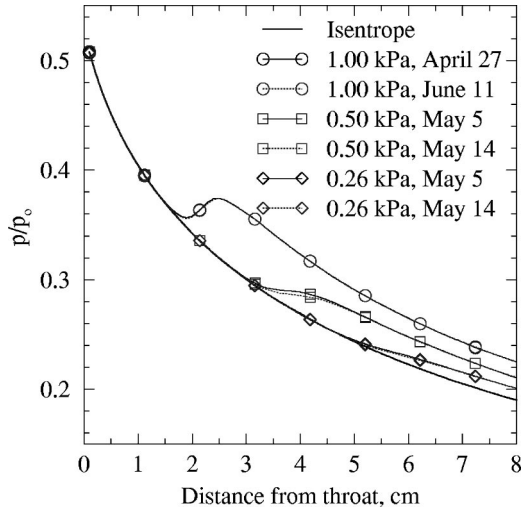


FIG. 3. The pressure traces for a series of water condensation experiments demonstrate that excellent repeatability is possible for the condensing flows.

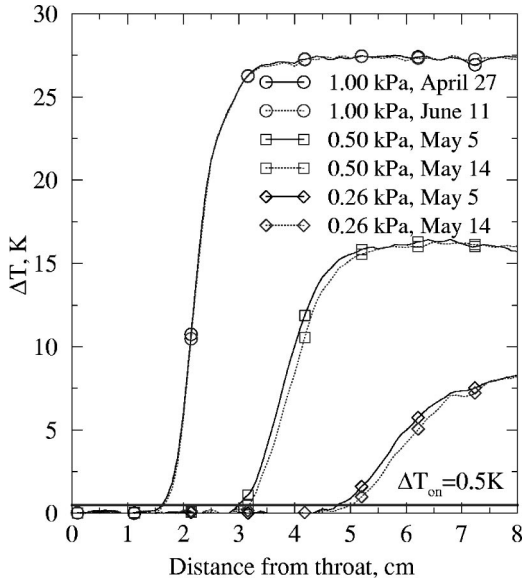


FIG. 4. The temperature difference between the condensing flow curve and the mixture isentrope corresponding to the pressure traces shown in Fig. 3. The line at 0.5 K is the onset criterion.

at onset, our calculations were performed using Eqs. (10) and (11), and the simplified Eq. (15). This simplified approach gave the same onset results (to three significant figures) as the more exact approach, but the latter, with Eqs. (12) and (17) in lieu of Eq. (15), should be used to obtain more accurate estimates of $T$ and $g$ further downstream.

The criteria used to determine onset vary,[18,20,40,41] and we now use a definition based on a constant temperature difference of 0.5 K between the condensing flow curve $T_{\mathrm{cf}}$ and the mixture isentrope $T_{\mathrm{mi}}$. Physically, this criterion corresponds roughly to a constant number of molecules condensed because most molecular fluids have similar molar heats of vaporization $\Delta H_{vap}$. For example, at their respective boiling points[42] $\Delta H_{vap}$ is 38.6 kJ/mol for ethanol, 41.4 kJ/mol for propanol, and 40.66 kJ/mol for water.

### C. Experimental reproducibility

Reproducing the operating conditions and the experimental results is extremely important, both for the onset experiments described here and in order to ensure that the results from SANS experiments conducted using the same equipment[15,16] can be interpreted. Because onset is defined in terms of a temperature difference between two expansions, reproducing the dry and condensing flow pressure traces is equally important. The temperature differences between any two $N_2$ isentropes can normally be kept to less than 0.1 K, a value that is only 20% of the onset criterion.

As demonstrated in the next three figures, excellent reproducibility is also possible for the condensing flows. Figure 3 shows six pressure traces for water condensation in the nozzle taken on four different days over a period of almost 2 months. The expansions all started at the same plenum pressure and temperature $(p_0, T_0)$ and on each occasion the nominal water partial pressures were 0.26, 0.5, and 1.0 kPa. The nozzle was not disassembled between these experiments. As illustrated in Fig. 3, the condensing flow curves follow a representative dry pressure trace closely up to the point of condensation. Each condensing flow curve then deviates in the expected manner; i.e., as the amount of condensible vapor is increased, onset occurs earlier in the nozzle and the deviation from the isentropic expansion increases. On the scale of Fig. 3 and for these water partial pressures, it is not possible to see the deviation between the pressure traces for the condensing and dry flows that was discussed earlier.

In Fig. 4, the difference between the temperature of the condensing flow curve and the mixture isentrope, $\Delta T = T_{\mathrm{cf}} - T_{\mathrm{mi}}$, is presented as a function of position in the nozzle for the water data in Fig. 3. The onset criterion $\Delta T = 0.5\,\mathrm{K}$ is clearly marked. The onset values $(p_{\mathrm{on}}, T_{\mathrm{on}})$ derived from these curves are the values of $p_v = p_{v0}(p/p_0)$ and $T$ along the condensing flow curve at the point where the value $\Delta T = 0.5\,\mathrm{K}$. If we make a Wilson plot with these data, as shown in Fig. 5, the excellent reproducibility of the experiments is again clearly demonstrated. Figure 5 also includes the equilibrium vapor pressure curve for subcooled liquid water[43] and onset data from other supersonic nozzle experiments. The supersaturations at onset for our experiments range from 25 to 450, and our onset observations are consistent with those of other researchers.[39,44] Finally, our experimental data points are well fit by a simple exponential function of temperature over this restricted temperature range. A model[20] that describes nucleation and growth in the nozzle shows the same behavior under these conditions although the predicted onset behavior is quantitatively different. The fit is only important because it is used later to interpolate a given data set for the onset pressure at a desired temperature.

## IV. EXPERIMENTAL RESULTS

### A. Wilson plots

The goal of most nucleation experiments is to measure the rate of particle formation as a function of supersaturation at constant temperature. In nozzles this is not yet possible, and phase transitions in nozzle experiments are still charac-

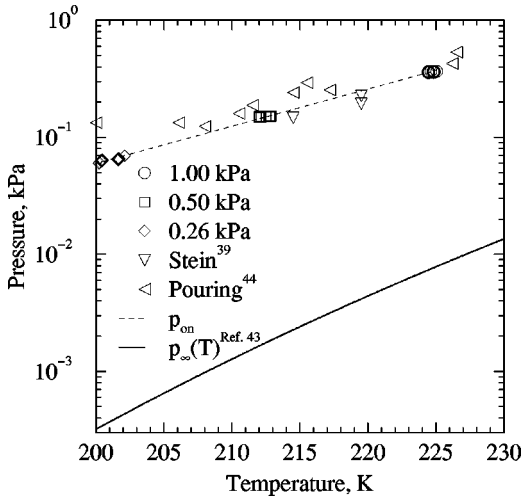


FIG. 5. The onset pressures and temperatures for water are presented on a Wilson plot and compared with other onset data from supersonic nozzle experiments. The vapor pressure line for the subcooled liquid is that of Wagner (see Ref. 43).

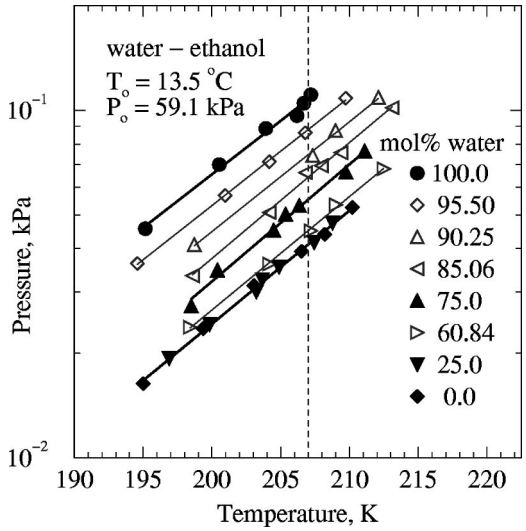


FIG. 7. A plot of the onset pressures for pure water, pure ethanol, and five intermediate mixtures. The data for 97.51 and 50.0 mol % water are not shown on the graph for reasons of clarity. All of the onset pressures and temperatures are given in Table II.

terized by the onset of condensation. In the water/ethanol/propanol experiments conducted here, we first examined the condensation behavior of the pure components. The values of $p_0$ and $T_0$ were fixed at $60.3 \pm 0.3$ kPa and $286.7 \pm 0.1$ K, and the liquid flow rates were adjusted so that the mole fraction of condensible vapor was in the range $5.0 \times 10^{-4} - 6.1 \times 10^{-3}$. Intermediate mixtures were then prepared, and for each intermediate mixture the mole fractions were varied in the same range. Although the plenum pressure was maintained at 60.3 kPa, we found from stagnation pressure measurements that there was a pressure drop of $1.2 \pm 0.1$ kPa across the mesh that holds the static pressure probe in place. Thus, the average stagnation pressure at the entrance to the nozzle was 59.1 kPa.

The data presented in this paper were measured during three different sessions over the course of a year (sessions A, B, and C). All of the ethanol–water and ethanol–propanol data come from the later sessions B and C. The water–propanol data were measured during sessions A and B. Between sessions A and B the nozzle was taken apart and reassembled, and the experimental procedure was refined. In particular, the balance used to characterize the flow through the nozzle was added to the system. Furthermore, onset data were taken over a wider temperature range starting in session B. The special problems associated with reconciling data from sessions A and B are discussed below in the context of

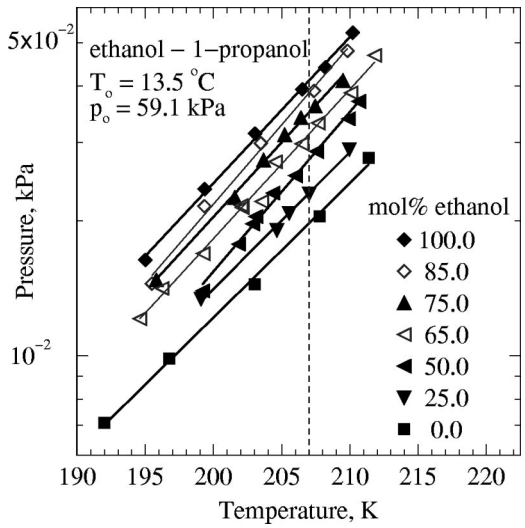


FIG. 6. A plot of the onset pressures for pure ethanol, pure propanol, and five intermediate mixtures. The data for 95.0 and 40.0 mol % ethanol are not shown on the graph for reasons of clarity. All of the onset pressures and temperatures are given in Table I.

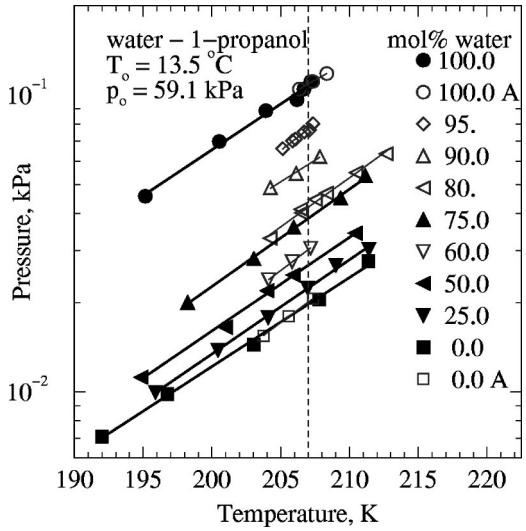


FIG. 8. A plot of the onset pressures for pure water, pure propanol, and seven intermediate mixtures. The data for 97.5, 39.9, and 20.0 mol % water are not shown on the graph for the sake of clarity. All of the onset pressures and temperatures are given in Table III.

TABLE I. Ethanol–propanol experimental conditions and results.

| Stagnation ($T_0 = 13.5 \pm 0.1$ °C) | | | Onset | | | | Stagnation ($T_0 = 13.5 \pm 0.1$ °C) | | | Onset | | | |
|---|---|---|---|---|---|---|---|---|---|---|---|---|---|
| $p_0$ (kPa) | $p_1$ (Pa) | $p_2$ (Pa) | $p/p_0$ | $p_1$ (Pa) | $p_2$ (Pa) | $T$ (K) | $p_0$ (kPa) | $p_1$ (Pa) | $p_2$ (Pa) | $p/p_0$ | $p_1$ (Pa) | $p_2$ (Pa) | $T$ (K) |
| 100 mol % ethanol | | | | | | | | | | | | | |
| 58.98±0.06 | 157.3 | ⋯ | 0.3345 | 52.6 | ⋯ | 210.2 | 59.14±0.05 | 39.6 | 21.3 | 0.2775 | 11.0 | 5.9 | 199.2 |
| 58.93±0.08 | 136.1 | ⋯ | 0.3235 | 44.0 | ⋯ | 208.2 | 59.09±0.06 | 34.9 | 18.8 | 0.2633 | 9.2 | 4.9 | 196.2 |
| 59.09±0.16 | 125.1 | ⋯ | 0.3145 | 39.4 | ⋯ | 206.5 | 59.15±0.06 | 30.8 | 16.6 | 0.2556 | 7.9 | 4.2 | 194.6 |
| 59.02±0.08 | 105.8 | ⋯ | 0.2965 | 31.4 | ⋯ | 203.1 | 50.0 mol % ethanol | | | | | | |
| 58.99±0.08 | 84.7 | ⋯ | 0.2780 | 23.6 | ⋯ | 199.3 | 59.04±0.04 | 54.8 | 54.9 | 0.3372 | 18.5 | 18.5 | 210.7 |
| 59.12±0.08 | 63.6 | ⋯ | 0.2574 | 16.4 | ⋯ | 195.0 | 59.01±0.03 | 50.8 | 50.8 | 0.3330 | 16.9 | 16.9 | 209.9 |
| 95.0 mol % ethanol | | | | | | | 59.02±0.03 | 44.6 | 44.6 | 0.3202 | 14.3 | 14.3 | 207.6 |
| 59.08±0.06 | 140.3 | 7.4 | 0.3302 | 46.3 | 2.4 | 209.4 | 59.06±0.03 | 40.4 | 40.5 | 0.3119 | 12.6 | 12.6 | 206.0 |
| 59.07±0.05 | 119.0 | 6.3 | 0.3174 | 37.8 | 2.0 | 207.0 | 59.07±0.03 | 38.1 | 38.1 | 0.3034 | 11.5 | 11.5 | 204.4 |
| 59.04±0.06 | 96.5 | 5.1 | 0.2958 | 28.5 | 1.5 | 202.9 | 59.03±0.03 | 34.5 | 34.5 | 0.2969 | 10.2 | 10.2 | 203.1 |
| 59.06±0.06 | 75.8 | 4.0 | 0.2771 | 21.0 | 1.1 | 199.2 | 58.99±0.03 | 33.3 | 33.3 | 0.2958 | 9.8 | 9.8 | 202.9 |
| 59.01±0.06 | 54.1 | 2.8 | 0.2498 | 13.5 | 0.7 | 193.3 | 59.09±0.03 | 30.6 | 30.6 | 0.2906 | 8.9 | 8.9 | 201.8 |
| 85.0 mol % ethanol | | | | | | | 58.99±0.03 | 25.2 | 25.2 | 0.2775 | 7.0 | 7.0 | 199.2 |
| 59.11±0.05 | 122.8 | 21.7 | 0.3322 | 40.8 | 7.2 | 209.8 | 40.0 mol % ethanol | | | | | | |
| 59.13±0.05 | 104.1 | 18.3 | 0.3191 | 33.2 | 5.9 | 207.4 | 59.07±0.08 | 51.5 | 77.1 | 0.3635 | 18.7 | 28.0 | 215.2 |
| 59.07±0.04 | 84.9 | 15.0 | 0.2986 | 25.4 | 4.5 | 203.5 | 59.06±0.10 | 43.7 | 65.6 | 0.3443 | 15.1 | 22.6 | 211.9 |
| 59.12±0.05 | 66.0 | 11.7 | 0.2779 | 18.3 | 3.2 | 199.3 | 59.09±0.07 | 38.4 | 57.6 | 0.3302 | 12.7 | 19.0 | 209.4 |
| 59.03±0.07 | 47.4 | 8.4 | 0.2597 | 12.3 | 2.2 | 195.5 | 59.05±0.09 | 35.7 | 53.5 | 0.3312 | 11.8 | 17.7 | 209.6 |
| 75.0 mol % ethanol | | | | | | | 59.06±0.08 | 28.1 | 42.1 | 0.3027 | 8.5 | 12.7 | 204.2 |
| 59.09±0.03 | 93.3 | 31.1 | 0.3307 | 30.9 | 10.3 | 209.5 | 59.07±0.12 | 28.0 | 42.0 | 0.3035 | 8.5 | 12.8 | 204.4 |
| 58.96±0.10 | 84.7 | 28.3 | 0.3195 | 27.1 | 9.0 | 207.4 | 59.02±0.11 | 20.1 | 30.1 | 0.2783 | 5.6 | 8.4 | 199.4 |
| 59.12±0.05 | 81.3 | 27.1 | 0.3140 | 25.5 | 8.5 | 206.4 | 59.07±0.13 | 17.7 | 26.5 | 0.2631 | 4.7 | 7.0 | 196.2 |
| 59.10±0.03 | 75.9 | 25.3 | 0.3076 | 23.3 | 7.8 | 205.2 | 25.0 mol % ethanol | | | | | | |
| 59.13±0.03 | 68.4 | 22.8 | 0.2997 | 20.5 | 6.8 | 203.7 | 58.97±0.05 | 26.5 | 79.6 | 0.3500 | 9.3 | 27.8 | 212.9 |
| 59.05±0.04 | 58.5 | 19.5 | 0.2890 | 16.9 | 5.6 | 201.6 | 59.00±0.06 | 21.7 | 65.0 | 0.3334 | 7.2 | 21.7 | 209.9 |
| 59.09±0.04 | 42.4 | 14.1 | 0.2611 | 11.1 | 3.7 | 195.8 | 59.03±0.03 | 18.1 | 54.4 | 0.3174 | 5.7 | 17.3 | 207.0 |
| 65.0 mol % ethanol | | | | | | | 59.05±0.05 | 16.8 | 50.5 | 0.3096 | 5.2 | 15.6 | 205.6 |
| 59.06±0.05 | 88.7 | 47.8 | 0.3436 | 30.5 | 16.4 | 211.8 | 59.00±0.03 | 15.6 | 46.9 | 0.3050 | 4.8 | 14.3 | 204.7 |
| 58.99±0.09 | 75.2 | 40.5 | 0.3341 | 25.1 | 13.5 | 210.1 | 59.03±0.05 | 12.1 | 36.3 | 0.2767 | 3.3 | 10.1 | 199.1 |
| 59.15±0.07 | 67.1 | 36.1 | 0.3208 | 21.5 | 11.6 | 207.7 | 100 mol % propanol | | | | | | |
| 59.07±0.05 | 61.5 | 33.1 | 0.3145 | 19.3 | 10.4 | 206.5 | 59.12±0.13 | ⋯ | 80.9 | 0.3413 | ⋯ | 27.6 | 211.4 |
| 59.14±0.05 | 58.0 | 31.2 | 0.3041 | 17.6 | 9.5 | 204.5 | 58.99±0.20 | ⋯ | 63.8 | 0.3216 | ⋯ | 20.5 | 207.8 |
| 59.06±0.06 | 48.1 | 25.9 | 0.2991 | 14.4 | 7.7 | 203.5 | 59.09±0.15 | ⋯ | 48.7 | 0.2965 | ⋯ | 14.4 | 203.0 |
| 59.13±0.04 | 48.3 | 26.0 | 0.2915 | 14.1 | 7.6 | 202.0 | 59.09±0.21 | ⋯ | 37.1 | 0.2658 | ⋯ | 9.9 | 196.7 |
| 59.10±0.13 | 47.8 | 25.7 | 0.2918 | 13.9 | 7.5 | 202.1 | 59.01±0.19 | ⋯ | 29.1 | 0.2437 | ⋯ | 7.1 | 192.0 |

understanding the water–propanol data. Although the system was disassembled between sessions B and C, the nozzle was not, and comparing data from these two sessions is straightforward. To distinguish between the measurement sessions, solid symbols are used for the data from session B, while open symbols are used for the data from session C (Figs. 6 and 7) or session A (Fig. 8).

Figures 6, 7, and 8 are the Wilson plots that correspond to the ethanol–propanol, water–ethanol, and water–propanol experiments, respectively. Based on an analysis of the measurement error we estimate that the uncertainty in $T_{on}$ is $\pm 1$ K while the uncertainty in $p_{on}$ is 5%. This analysis precludes any systematic bias which may still be inherent in the experimental procedure. Tables I, II, and III summarize the values of $p_0$, $T_0$, and $y$ for each experiment as well as the corresponding values of $p_{on}$ and $T_{on}$. For the purposes of modeling the onset data, the value of $d(A/A^*)/dx$ in the linear part of the expansion was $0.0495 \pm 0.001\ \mathrm{cm}^{-1}$ during sessions A, B, and C.

We begin our discussion of the Wilson plots by examining the ethanol–propanol data. Ethanol and propanol form ideal liquid mixtures, and their surface tensions do not differ significantly. In this case the total condensible vapor pressure required to maintain a constant nucleation rate at a fixed temperature for an intermediate mixture should vary linearly between the values for the pure components. This linear behavior was observed for ethanol–hexanol mixtures both experimentally[30] and theoretically.[30,45] If the isothermal onset criterion in our experiments corresponds to roughly the same particle formation history, one would expect that the total condensible pressure at constant onset temperature should also interpolate linearly between the values of the pure components for the intermediate mixtures. As illustrated in Fig. 6, the onset curves for the ethanol–propanol mixtures are fairly evenly spaced as a function of composition between the onset curves for the pure components. For example, the total pressure of condensible vapor required to produce onset in a 50 mol % mixture lies about halfway between the pressures required for the pure components. In contrast, for the water–ethanol data in Fig. 7, the onset curve for a 25 mol % water–ethanol mixture is indistinguishable from the pure ethanol curve and even the 60 mol % water–ethanol mixture is extremely close to the pure ethanol curve. For the water rich curves, on the other hand, the addition

TABLE II. Water–ethanol experimental conditions and results.

| Stagnation ($T_0=13.5\pm0.1$ °C) | | | Onset | | | | Stagnation ($T_0=13.5\pm0.1$ °C) | | | Onset | | | |
|---|---|---|---|---|---|---|---|---|---|---|---|---|---|
| $p_0$ (kPa) | $p_1$ (Pa) | $p_2$ (Pa) | $p/p_0$ | $p_1$ (Pa) | $p_2$ (Pa) | $T$ (K) | $p_0$ (kPa) | $p_1$ (Pa) | $p_2$ (Pa) | $p/p_0$ | $p_1$ (Pa) | $p_2$ (Pa) | $T$ (K) |
| 100 mol % water | | | | | | | | | | | | | |
| 59.07±0.07 | 348.5 | ⋯ | 0.3186 | 111.1 | ⋯ | 207.2 | 59.02±0.04 | 121.9 | 40.6 | 0.3088 | 37.7 | 12.5 | 205.3 |
| 59.10±0.03 | 331.6 | ⋯ | 0.3162 | 104.9 | ⋯ | 206.7 | 58.96±0.03 | 111.4 | 37.2 | 0.3043 | 33.9 | 11.3 | 204.5 |
| 58.99±0.03 | 307.7 | ⋯ | 0.3135 | 96.5 | ⋯ | 206.2 | 58.97±0.11 | 91.8 | 30.6 | 0.2836 | 26.0 | 8.7 | 200.4 |
| 58.92±0.12 | 294.1 | ⋯ | 0.3016 | 88.7 | ⋯ | 203.9 | 59.04±0.06 | 74.9 | 24.9 | 0.2743 | 20.5 | 6.8 | 198.5 |
| 59.14±0.05 | 245.6 | ⋯ | 0.2843 | 69.8 | ⋯ | 200.5 | 60.84 mol % water | | | | | | |
| 59.15±0.06 | 176.8 | ⋯ | 0.2584 | 45.7 | ⋯ | 195.2 | 59.08±0.05 | 118.7 | 76.4 | 0.3479 | 41.3 | 26.6 | 212.5 |
| 97.51 mol % water | | | | | | | 59.15±0.07 | 99.2 | 63.8 | 0.3285 | 32.6 | 21.0 | 209.0 |
| 59.07±0.05 | 329.4 | 8.4 | 0.3302 | 108.8 | 2.8 | 209.3 | 59.17±0.05 | 86.0 | 55.4 | 0.3186 | 27.4 | 17.6 | 207.2 |
| 59.12±0.05 | 284.4 | 7.3 | 0.3138 | 89.2 | 2.3 | 206.2 | 59.08±0.07 | 72.6 | 46.7 | 0.3026 | 22.0 | 14.1 | 204.2 |
| 59.08±0.06 | 238.7 | 6.1 | 0.2979 | 71.1 | 1.8 | 203.2 | 59.11±0.06 | 52.8 | 34.0 | 0.2738 | 14.5 | 9.3 | 198.4 |
| 59.09±0.06 | 221.0 | 5.7 | 0.2874 | 63.5 | 1.6 | 201.2 | 50.0 mol % water | | | | | | |
| 59.10±0.05 | 201.5 | 5.2 | 0.2846 | 57.4 | 1.5 | 200.6 | 58.96±0.06 | 90.6 | 90.6 | 0.3422 | 31.0 | 31.0 | 211.5 |
| 59.08±0.05 | 146.8 | 3.8 | 0.2557 | 37.5 | 1.0 | 194.6 | 59.00±0.07 | 80.3 | 80.3 | 0.3338 | 26.8 | 26.8 | 210.0 |
| 95.50 mol % water | | | | | | | 59.14±0.06 | 71.4 | 71.4 | 0.3207 | 22.9 | 22.9 | 207.6 |
| 59.09±0.05 | 311.0 | 14.7 | 0.3327 | 103.5 | 4.9 | 209.7 | 59.07±0.08 | 61.8 | 61.8 | 0.3101 | 19.2 | 19.2 | 205.6 |
| 59.10±0.06 | 260.1 | 12.3 | 0.3167 | 82.4 | 3.9 | 206.8 | 59.02±0.07 | 52.3 | 52.4 | 0.2933 | 15.3 | 15.4 | 202.3 |
| 59.01±0.5 | 224.5 | 10.6 | 0.3028 | 68.0 | 3.2 | 204.2 | 59.00±0.06 | 42.7 | 42.8 | 0.2791 | 11.9 | 11.9 | 199.5 |
| 59.05±0.5 | 190.0 | 8.9 | 0.2864 | 54.4 | 2.6 | 200.9 | 59.15±0.05 | 33.5 | 33.5 | 0.2552 | 8.5 | 8.6 | 194.5 |
| 59.05±0.05 | 135.5 | 6.4 | 0.2557 | 34.6 | 1.6 | 194.6 | 25.0 mol % water | | | | | | |
| 90.25 mol % water | | | | | | | 59.12±0.05 | 36.3 | 108.8 | 0.3270 | 11.9 | 35.6 | 208.8 |
| 59.06±0.07 | 284.5 | 30.7 | 0.3460 | 98.4 | 10.6 | 212.1 | 59.13±0.05 | 32.6 | 97.8 | 0.3197 | 10.4 | 31.3 | 207.4 |
| 59.09±0.07 | 240.4 | 26.0 | 0.3285 | 79.0 | 8.5 | 209.0 | 59.10±0.06 | 28.9 | 86.7 | 0.3062 | 8.9 | 26.6 | 204.9 |
| 58.99±0.07 | 209.2 | 22.6 | 0.3195 | 66.9 | 7.2 | 207.3 | 59.13±0.05 | 27.2 | 81.6 | 0.2998 | 8.2 | 24.5 | 203.7 |
| 59.07±0.06 | 134.6 | 14.5 | 0.2754 | 37.1 | 4.0 | 198.7 | 59.13±0.04 | 25.3 | 75.9 | 0.2976 | 7.5 | 22.6 | 203.2 |
| 85.06 mol % water | | | | | | | 59.07±0.05 | 21.6 | 64.8 | 0.2805 | 6.1 | 18.2 | 199.8 |
| 59.08±0.04 | 246.1 | 43.3 | 0.3517 | 86.5 | 15.2 | 213.1 | 59.14±0.04 | 18.2 | 54.5 | 0.2663 | 4.8 | 14.5 | 196.9 |
| 59.11±0.05 | 194.5 | 34.2 | 0.3306 | 64.3 | 11.3 | 209.4 | 59.09±0.95 | 14.4 | 43.3 | 0.2465 | 3.6 | 10.7 | 192.6 |
| 59.14±0.05 | 182.7 | 32.1 | 0.3228 | 59.0 | 10.4 | 207.9 | 100 mol % ethanol | | | | | | |
| 59.00±0.05 | 177.9 | 31.2 | 0.3167 | 56.3 | 9.9 | 206.8 | 58.98±0.06 | ⋯ | 157.3 | 0.3345 | ⋯ | 52.6 | 210.2 |
| 59.22±0.09 | 142.8 | 25.1 | 0.3028 | 43.2 | 7.6 | 204.2 | 58.93±0.08 | ⋯ | 136.1 | 0.3235 | ⋯ | 44.0 | 208.2 |
| 59.11±0.05 | 103.6 | 18.2 | 0.2746 | 28.4 | 5.0 | 198.6 | 59.09±0.16 | ⋯ | 125.1 | 0.3145 | ⋯ | 39.4 | 206.5 |
| 75.0 mol % water | | | | | | | 59.02±0.08 | ⋯ | 105.8 | 0.2965 | ⋯ | 31.4 | 203.1 |
| 58.95±0.08 | 168.3 | 56.1 | 0.3403 | 57.3 | 19.1 | 211.1 | 58.99±0.08 | ⋯ | 84.7 | 0.2780 | ⋯ | 23.6 | 199.3 |
| 59.10±0.05 | 149.8 | 49.9 | 0.3327 | 49.9 | 16.6 | 209.7 | 59.12±0.08 | ⋯ | 63.6 | 0.2574 | ⋯ | 16.4 | 195.0 |
| 59.02±0.12 | 127.1 | 42.4 | 0.3142 | 39.9 | 13.3 | 206.3 | | | | | | | |

of as little as 5 mol % ethanol significantly decreases the total pressure of condensible vapor required to achieve onset at a given temperature. A similar trend is apparent in the water–propanol data illustrated in Fig. 8.

At this point it is important to discuss the difficulties associated with reconciling the data from sessions A and B that comprise the water–propanol data set given in Fig. 8. During session A, when the LN2 balance was not yet available, the partial pressures of the components in the gas mixture were calculated using $\dot{m}^0_{N_2}=\rho^* u^* A^*$, where $A^*$ was the design value. During session B, the molar flow rate of $N_2$ through the nozzle was carefully measured and the experimental value of $\dot{m}^0_{N_2}$ was used to calculate the gas phase composition. When the onset pressures for the pure components measured during sessions A and B were initially compared, the pressures from session A were distinctly higher than those from session B. Furthermore, the intermediate mixtures did not exhibit the monotonic increase in total pressure with increasing water content that we observed in the water–ethanol data. In light of the excellent agreement observed during our repeatability experiments for pure water (see Fig. 5), the discrepancy between the pure component onset curves measured in sessions A and B was both unacceptable and unphysical. Because nothing else changed in the experimental procedure, the source of the discrepancy had to be the difference between the design value of $A^*$ and its true, but unknown, value during session A. The measured value of $\dot{m}^0_{N_2}$ from session B was not an appropriate choice, because the nozzle had been cleaned and reassembled between the two sessions. Experiments involving repeated nozzle assembly demonstrated that the value of $\dot{m}^0_{N_2}$ can vary by as much as 15% unless careful assembly protocols are observed. Increasing the value of $\dot{m}^0_{N_2}$ for session A to account for a different $A^*$, however, gave excellent agreement between the two pure water data sets. The $\dot{m}^0_{N_2}$ for session A appears to have been 6% higher than the value measured during session B. The increase in $A^*$ and $\dot{m}^0_{N_2}$ correspond to an additional separation between the top and bottom nozzle blocks of only 0.3 mm. Although the throat area was apparently different for the nozzle assembly during session A, the expansion rates were indistinguishable. Hence, once properly scaled, the data from session A should be perfectly compatible with the data from sessions B and C. Applying this correction to the remaining data from session A, we found

TABLE III. Water–propanol experimental conditions and results.

| Stagnation ($T_0=13.5\pm0.1$ °C) | | | Onset | | | | Stagnation ($T_0=13.5\pm0.1$ °C) | | | Onset | | | |
|---|---|---|---|---|---|---|---|---|---|---|---|---|---|
| $p_0$ (kPa) | $p_1$ (Pa) | $p_2$ (Pa) | $p/p_0$ | $p_1$ (Pa) | $p_2$ (Pa) | $T$ (K) | $p_0$ (kPa) | $p_1$ (Pa) | $p_2$ (Pa) | $p/p_0$ | $p_1$ (Pa) | $p_2$ (Pa) | $T$ (K) |
| 100 mol % water | | | | | | | 75.0 mol % water | | | | | | |
| 59.33±0.03 | 363.9 | ··· | 0.3250 | 118.3 | ··· | 208.3 | 59.00±0.07 | 133.1 | 44.4 | 0.3526 | 46.9 | 15.6 | 213.3 |
| 59.29±0.02 | 347.9 | ··· | 0.3195 | 111.2 | ··· | 207.3 | 59.01±0.06 | 117.8 | 39.3 | 0.3406 | 40.1 | 13.4 | 211.2 |
| 59.07±0.07 | 348.5 | ··· | 0.3186 | 111.1 | ··· | 207.2 | 59.08±0.09 | 102.2 | 34.1 | 0.3305 | 33.8 | 11.3 | 209.3 |
| 59.10±0.03 | 331.6 | ··· | 0.3162 | 104.9 | ··· | 206.7 | 58.97±0.07 | 86.2 | 28.7 | 0.3120 | 26.9 | 9.0 | 205.9 |
| 59.26±0.03 | 333.2 | ··· | 0.3142 | 104.7 | ··· | 206.3 | 59.11±0.06 | 71.0 | 23.7 | 0.2969 | 21.1 | 7.0 | 203.1 |
| 58.99±0.03 | 307.7 | ··· | 0.3135 | 96.5 | ··· | 206.2 | 59.01±0.05 | 55.1 | 18.3 | 0.2729 | 15.0 | 5.0 | 198.2 |
| 58.92±0.12 | 294.1 | ··· | 0.3016 | 88.7 | ··· | 203.9 | 60.0 mol % water | | | | | | |
| 59.14±0.05 | 245.6 | ··· | 0.2843 | 69.8 | ··· | 200.5 | 59.23±0.03 | 57.6 | 38.4 | 0.3188 | 18.3 | 12.2 | 207.2 |
| 59.15±0.06 | 176.8 | ··· | 0.2584 | 45.7 | ··· | 195.2 | 59.13±0.04 | 52.9 | 35.3 | 0.3116 | 16.5 | 11.0 | 205.8 |
| 97.5 mol % water | | | | | | | 59.28±0.04 | 47.4 | 31.6 | 0.3027 | 14.3 | 9.6 | 204.1 |
| 59.25±0.02 | 288.1 | 7.4 | 0.3211 | 92.5 | 2.4 | 207.6 | 50.0 mol % water | | | | | | |
| 59.22±0.02 | 275.1 | 7.0 | 0.3165 | 87.1 | 2.2 | 206.7 | 59.22±0.20 | 50.9 | 50.9 | 0.3363 | 17.1 | 17.1 | 210.4 |
| 59.07±0.08 | 248.4 | 6.4 | 0.3081 | 76.5 | 2.0 | 205.1 | 59.07±0.06 | 39.8 | 39.8 | 0.3117 | 12.4 | 12.4 | 205.9 |
| 95 mol % water | | | | | | | 59.20±0.05 | 36.4 | 36.4 | 0.3018 | 11.0 | 11.0 | 204.0 |
| 59.22±0.03 | 238.1 | 12.5 | 0.3199 | 76.2 | 4.0 | 207.3 | 59.22±0.20 | 28.9 | 28.9 | 0.2861 | 8.3 | 8.3 | 201.0 |
| 59.27±0.03 | 227.4 | 12.0 | 0.3186 | 72.4 | 3.8 | 207.1 | 59.16±0.07 | 21.9 | 21.9 | 0.2569 | 5.6 | 5.6 | 194.8 |
| 59.19±0.04 | 225.9 | 11.9 | 0.3162 | 71.4 | 3.8 | 206.7 | 39.9 mol % water | | | | | | |
| 59.26±0.03 | 215.8 | 11.3 | 0.3130 | 67.5 | 3.5 | 206.1 | 59.25±0.06 | 31.0 | 46.9 | 0.3208 | 9.9 | 15.0 | 207.7 |
| 59.15±0.05 | 213.6 | 11.2 | 0.3119 | 66.6 | 3.5 | 205.8 | 59.28±0.03 | 29.0 | 43.8 | 0.3130 | 9.1 | 13.7 | 206.2 |
| 59.28±0.03 | 203.6 | 10.7 | 0.3081 | 62.7 | 3.3 | 205.1 | 59.41±0.03 | 27.1 | 40.7 | 0.3067 | 8.3 | 12.5 | 205.0 |
| 90.0 mol % water | | | | | | | 25.0 mol % water | | | | | | |
| 59.32±0.03 | 173.3 | 19.3 | 0.3222 | 55.9 | 6.2 | 207.8 | 59.07±0.03 | 22.2 | 66.5 | 0.3418 | 7.6 | 22.7 | 211.4 |
| 59.24±0.06 | 156.9 | 17.4 | 0.3130 | 49.1 | 5.5 | 206.1 | 59.06±0.04 | 20.4 | 61.2 | 0.3283 | 6.7 | 20.1 | 209.0 |
| 59.35±0.04 | 144.7 | 16.1 | 0.3032 | 43.9 | 4.9 | 204.2 | 59.05±0.03 | 17.7 | 53.1 | 0.3171 | 5.6 | 16.8 | 206.9 |
| 80.0 mol % water | | | | | | | 59.05±0.03 | 14.7 | 44.3 | 0.3021 | 4.5 | 13.4 | 204.1 |
| 59.27±0.03 | 145.0 | 36.9 | 0.3490 | 50.6 | 12.9 | 212.7 | 59.12±0.03 | 12.2 | 36.6 | 0.2835 | 3.5 | 10.4 | 200.4 |
| 59.30±0.02 | 130.1 | 32.8 | 0.3366 | 43.8 | 11.1 | 210.5 | 59.10±0.04 | 9.5 | 28.6 | 0.2620 | 2.5 | 7.5 | 195.9 |
| 59.25±0.02 | 115.0 | 29.1 | 0.3248 | 37.3 | 9.5 | 208.3 | 20.0 mol % water | | | | | | |
| 59.09±0.02 | 110.7 | 27.7 | 0.3215 | 35.6 | 8.9 | 207.5 | 59.24±0.06 | 13.4 | 53.8 | 0.3184 | 4.3 | 17.1 | 207.1 |
| 59.33±0.03 | 104.8 | 26.2 | 0.3151 | 33.0 | 8.3 | 206.4 | 59.23±0.06 | 12.8 | 51.0 | 0.3147 | 4.0 | 16.1 | 206.5 |
| 59.22±0.03 | 101.3 | 25.9 | 0.3150 | 31.9 | 8.1 | 206.5 | 59.29±0.06 | 12.0 | 48.0 | 0.3069 | 3.7 | 14.7 | 205.0 |
| 59.14±0.03 | 86.6 | 22.2 | 0.3029 | 26.2 | 6.7 | 204.2 | 59.20±0.05 | 11.1 | 44.5 | 0.3044 | 3.4 | 13.5 | 204.5 |

that the two pure propanol data sets now agreed extremely well. Furthermore, the behavior of the intermediate mixtures was consistent with the behavior observed for water–ethanol. Finally, we note that four of the seven data points from the 80 mol % water–20 mol % propanol data set were obtained using separate vapor generators for the water and propanol. As expected, no systematic difference is observed between the onset values determined using two generators and those determined using a single generator.

### B. Critical pressure plots

In binary nucleation experiments it is convenient to summarize the nucleation behavior in terms of a critical activity plot. Such a plot shows the activity pairs that correspond to a chosen nucleation rate at a constant temperature. The plots are useful because they clearly illustrate how much the binary nucleation process is affected relative to the nucleation of either pure component. Because onset is a strong function of the particle formation rate, an equally useful plot for the nozzle data is one that shows the pressures or activities corresponding to the onset of condensation at constant temperature. If the experiments are all conducted in the same nozzle, starting from the same $p_0$ and $T_0$, a constant onset temperature implies onset at the same location in the nozzle. Thus, the experiments all have the same gasdynamic history upstream of condensation. It is important to note that although the gasdynamic history is the same, the particle formation process is not. Thus, the aerosols formed under conditions of constant onset will differ in terms of particle number concentration, size, and width of the size distribution. Until we can measure nucleation rates directly in the nozzle, isothermal onset plots are the best available analogs of critical activity plots.

Figure 9 summarizes the partial pressure pairs that correspond to onset at 207 K. For our nozzle under the current stagnation conditions, $T_{on}=207$ K occurs approximately 2.5 cm downstream of the throat at a Mach number of 1.39. The values of $p_{on}$ presented in Fig. 9 are derived from the exponential fits to the data in Figs. 6–8. For each data set in Fig. 9, the vertical axis corresponds to the species with the higher pure component onset pressure. For the water–alcohol mixtures, water has the higher onset pressure while for the ethanol–propanol mixtures, ethanol has the higher onset pressure. The data are presented as partial pressure pairs rather than activity pairs because pressure is the measured quantity. Furthermore, in our case determining activity requires extrapolating the equilibrium vapor pressure curves to extremely low temperatures. Even if the extrapolated values were valid, the activity plots would have essentially the same

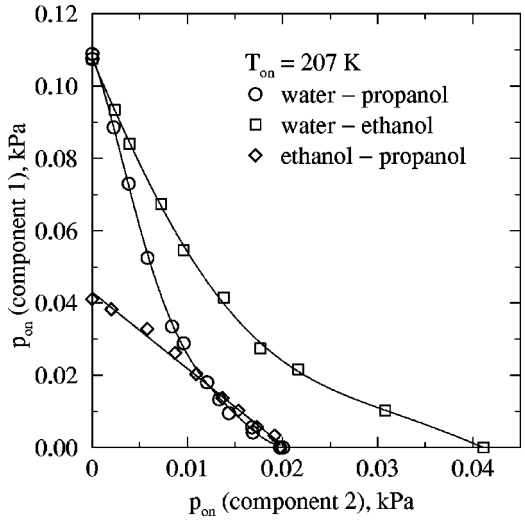


FIG. 9. The partial pressures corresponding to onset at 207 K for ethanol–propanol vary almost linearly between the pure component values. In contrast, the water–ethanol and water–propanol data are significantly bowed toward lower pressures. The solid lines are fits to guide the eye.

shape as the pressure plots shown here, because under isothermal conditions each partial pressure is divided by a constant value.

In Fig. 9 the water–ethanol and water–propanol partial pressures all lie distinctly below a straight line joining the pure components. Under less severe conditions,[10,31,33] water–alcohol critical activity plots exhibit very similar behavior, and both results suggest there is a strong mutual enhancement in the particle formation process involving the two species. In contrast, the ethanol–propanol data points all lie close to a straight line joining the pure component values. In their ethanol–hexanol binary nucleation experiments, Strey and Viisanen[30] also observed this ideal behavior in the critical activity plots for their mixture of two straight chain alcohols.

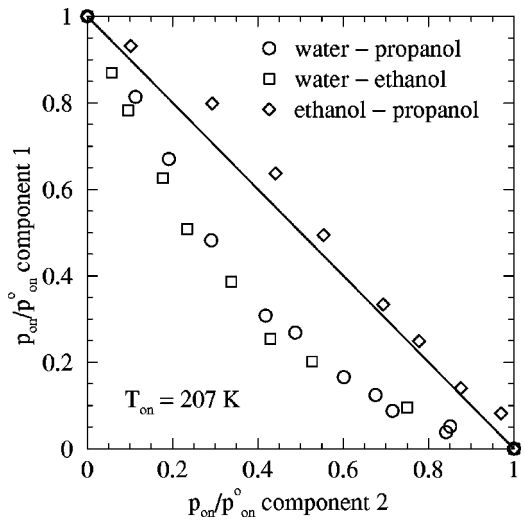


FIG. 10. The partial pressures from Fig. 9 are normalized by the partial pressure at onset for the corresponding pure component $p^0_{on}$. Normalized partial pressures are equivalent to normalized activities because the equilibrium vapor pressure cancels. The common scale accentuates the difference between the rather ideal behavior of the ethanol–propanol mixtures and the nonideal behavior of the water–alcohol mixtures.

To collapse all of the data onto a common scale, we normalized the data in Fig. 9 by dividing each partial pressure by the onset pressure of the corresponding pure component. These normalized pressures, illustrated in Fig. 10, are equivalent to the normalized activities used by Strey *et al.*[33] because in normalizing each activity by the value for the pure component the equilibrium vapor pressure cancels. Again, the rather ideal behavior of the alcohol–acohol mixtures stands in stark contrast to the behavior of the nonideal aqueous alcohol systems. The major qualitative difference between our results and those of Strey *et al.*[33] is that we do not see a substantial difference between ethanol and propanol on the scaled figure, whereas they observed a strong systematic decrease in enhancement as the chain length of the alcohol increases.

## V. SUMMARY AND CONCLUSIONS

We have developed a reliable supersonic nozzle apparatus to systematically investigate both unary and binary condensation. The reproducibility of the experimental data is good, and both miscible and partially miscible systems can be investigated. The current work examined condensation in the water–ethanol, water–propanol, and ethanol–propanol binary systems. In the ethanol–propanol system, the isothermal onset pressure for the intermediate mixtures varied almost linearly between the onset pressures for the pure components. This behavior is consistent with the observations of Strey and Viisanen[30] who found that the activities required to maintain constant nucleation rate under isothermal conditions varied linearly between the pure component values in the ideal ethanol–hexanol system. In the nonideal water–alcohol mixtures we observed a large reduction in the total pressure required to maintain isothermal onset in the nozzle over that predicted by linear interpolation between the endpoints. Again, this is consistent with results observed at lower nucleation rates. Those results can be rationalized in terms of surface enrichment, a concept supported by recent molecular dynamics simulations on ethanol–water clusters.[46] In the present case, the explanation may be more complicated because condensation onset is not determined solely by nucleation. Droplet growth also plays an important, and sometimes dominant, role.[47] In the future we hope to complement these conventional experiments with SANS measurements to better constrain models of particle formation and growth in supersonic nozzles.

## ACKNOWLEDGMENTS

This work was supported by the National Science Foundation, Division of Chemistry under Grants No. CHE-9502604 (B.E.W.), CHE-9522127 (B.E.W.), and CHE-9729274 (B.E.W.), by the Donors of the Petroleum Research Fund administered by the American Chemical Society, and by the Engineering Sciences Program of the Division of Materials Sciences and Engineering, Basic Energy Sciences, U.S. Department of Energy (G.W.).

## APPENDIX: GAS STREAM COMPOSITION

Here, we develop an expression that allows us to calculate the composition of the gas stream using only the measured flow rates of condensible species and the measured flow rate of dry carrier gas at the same stagnation conditions as for the mixed gas stream. The total mole fraction of condensible vapor $y$ in the gas stream before any condensation has occurred is defined by Eq. (1) as

$$y=\frac{\dot{m}_v/\mu_v}{\dot{m}_T/\mu}, \tag{A1}$$

where $\dot{m}_v$ and $\mu_v$ are the total mass flow rate and the mean molecular weight of the condensible vapor, respectively, $\dot{m}_T$ and $\mu$ are the mass flow rate and the mean molecular weight for the total gas stream,

$$\mu=(1-y)\mu_i+y\mu_v, \tag{A2}$$

and

$$\mu_v=\sum_\alpha y_\alpha\mu_\alpha/y. \tag{A3}$$

In Eq. (A3), the subscript $\alpha$ denotes a condensible vapor species, i.e., the sum on $\alpha$, here and below, does not include the carrier gas. Once $y$ is known to sufficient accuracy, the individual $y_\alpha$ values may be easily found using the equations

$$y_\alpha=y\frac{\dot{m}_\alpha/\mu_\alpha}{\dot{m}_v/\mu_v}, \tag{A4}$$

and

$$\dot{m}_v/\mu_v=\sum_\alpha \dot{m}_\alpha/\mu_\alpha. \tag{A5}$$

To proceed we first recall that $\dot{m}_T$ is determined at the nozzle throat by the continuity equation, Eq. (9),

$$\dot{m}_T=\rho^*u^*A^*. \tag{A6}$$

Starred quantities are evaluated at the throat. The analysis of this equation is facilitated by the use of the following relationships that are valid for ideal gas mixtures and isentropic expansions:

$$\rho^*=\rho_0\left[\frac{1+\gamma_m}{2}\right]^{1/(1-\gamma_m)}, \tag{A7}$$

$$u^*=\sqrt{\gamma_m RT_m^*/\mu}, \tag{A8}$$

$$T_m^*/T^*=(1+\gamma_m)/(1+\gamma), \tag{A9}$$

$$\rho_0=\frac{\mu p_0}{RT_0}, \tag{A10}$$

where $\gamma_m$ is defined by Eq. (7), $T_m^*$ and $T^*$ are the gas temperatures of the mixture and the dry carrier gas, respectively, and $\rho_0$ is the stagnation density of the mixture. Using these equations, we can exactly rewrite Eq. (A6) as

$$\dot{m}_T=\dot{m}_i^0(\mu/\mu_i)f(y), \tag{A11}$$

where $\dot{m}_i^0$ is the mass flow rate for dry carrier gas at the same stagnation pressure and temperature, $p_0$ and $T_0$, as the mixture, and

$$f(y)=\left[\frac{[(1+\gamma_m)/2]^{(3-\gamma_m)/(1-\gamma_m)}}{[(1+\gamma)/2]^{(3-\gamma)/(1-\gamma)}}\frac{\gamma_m\mu_i}{\gamma\mu}\right]^{1/2}. \tag{A12}$$

If we now substitute Eq. (A11) into Eq. (A1), expand $f(y)$ to first order in $y$, and solve the resulting expression for $y$, we obtain

$$y=y^0/(1-dy^0), \tag{A13}$$

where

$$y^0=\frac{\dot{m}_v/\mu_v}{\dot{m}_i^0/\mu_i}, \tag{A14}$$

$$d=\frac{1}{2}\left[\frac{\mu_v}{\mu_i}-1+\frac{\Delta C_p}{C_{pi}}\left(\frac{2\gamma}{\gamma-1}\ln\frac{1+\gamma}{2}+\frac{2\gamma(\gamma-1)}{1+\gamma}-1\right)\right], \tag{A15}$$

$$\Delta C_p=\overline{C}_{pv}-C_{pi}, \tag{A16}$$

and

$$\overline{C}_{pv}=\frac{\Sigma_\alpha\dot{m}_\alpha C_{p\alpha}/\mu_\alpha}{\dot{m}_v/\mu_v}. \tag{A17}$$

A first order expansion for $f(y)$ is sufficient because $y$ is generally less than 0.02. For $N_2$ carrier gas, $\gamma=1.4$, and Eq. (A15) simplifies to

$$d=\frac{1}{2}\left[\frac{\mu_v}{\mu_i}-1+0.743\frac{\Delta C_p}{C_{pi}}\right], \tag{A18}$$

so that the coefficient $d$ can be readily determined from the relative composition of the condensible vapor and the known molecular weights and heat capacities of the pure vapor species. For the gas mixtures of interest here, $d$ is always positive, and $y^0$ slightly underestimates $y$.


[1] R. H. Heist and H. He, J. Phys. Chem. Ref. Data **23**, 781 (1994).
[2] M. M. Rudek, J. L. Katz, and H. Uchtmann, J. Chem. Phys. **110**, 11505 (1999).
[3] R. H. Heist, J. Ahmed, and M. Janjua, J. Phys. Chem. **98**, 4443 (1994).
[4] D. Kane and M. S. El-Shall, J. Chem. Phys. **105**, 7617 (1996).
[5] V. Vohra and R. H. Heist, J. Chem. Phys. **104**, 382 (1996).
[6] M. P. Anisimov, J. A. Koropchak, A. G. Nasibulin, and L. V. Timoshina, J. Chem. Phys. **109**, 10004 (1998).
[7] R. Strey, P. Wagner, and Y. Viisanen, J. Phys. Chem. **98**, 7748 (1994).
[8] G. W. Adams, J. L. Schmitt, and R. A. Zalabsky, J. Chem. Phys. **81**, 5074 (1984).
[9] F. Peters and B. Paikert, Exp. Fluids **7**, 521 (1989).
[10] T. Rodemann and F. Peters, J. Chem. Phys. **105**, 5168 (1996).
[11] K. N. H. Looijmans, P. C. Kreisels, and M. E. H. van Dongen, Exp. Fluids **15**, 61 (1993).
[12] K. N. H. Looijmans and M. E. H. van Dongen, Exp. Fluids **23**, 54 (1997).
[13] B. E. Wyslouzil, J. H. Seinfeld, R. C. Flagan, and K. Okuyama, J. Chem. Phys. **94**, 6827 (1991).
[14] B. E. Wyslouzil, J. H. Seinfeld, R. C. Flagan, and K. Okuyama, J. Chem. Phys. **94**, 6842 (1991).
[15] B. E. Wyslouzil, J. L. Cheung, G. Wilemski, and R. Strey, Phys. Rev. Lett. **79**, 431 (1997).
[16] B. E. Wyslouzil, G. Wilemski, J. L. Cheung, R. Strey, and J. Barker, Phys. Rev. E **60**, 4330 (1999).
[17] K. Liu, J. D. Cruzan, and R. J. Saykally, Science **271**, 929 (1996).
[18] P. P. Wegener ''Gasdynamics of expansion flows with condensation and homogeneous nucleation of water vapor,'' in *Nonequilibrium Flows*, Gasdynamics, Part I, Vol. 1, edited by P. P. Wegener (Marcel Dekker, New York, 1966).

[19] H. W. Liepmann and A. Roshko, *Elements of Gasdynamics* (Wiley, New York, 1957).
[20] B. E. Wyslouzil, G. Wilemski, M. G. Beals, and M. B. Frish, Phys. Fluids **6**, 2845 (1994).
[21] G. D. Stein and C. A. Moses, J. Colloid Interface Sci. **39**, 504 (1972).
[22] C. A. Moses and G. D. Stein, J. Fluids Eng. **100**, 311 (1978).
[23] B. J. C. Wu, P. P. Wegener, and G. D. Stein, J. Chem. Phys. **69**, 1776 (1978).
[24] C. H. Heath, K. A. Streletzky, J. Wölk, B. E. Wyslouzil, and R. Strey, in *Nucleation and Atmospheric Aerosols, 2000*, edited by B. N. Hale and M. Kulmala (American Institute of Physics, New York, 2000) p. 59.
[25] C. H. Heath, K. A. Streletzky, B. E. Wyslouzil, and G. Wilemski, in *Nucleation and Atmospheric Aerosols, 2000*, edited by B. Hale and M. Kulmala (American Institute of Physics, New York, 2000) p. 63.
[26] H. Flood, Z. Phys. Chem. **A170**, 286 (1934).
[27] P. Mirabel and J. L. Katz, J. Chem. Phys. **67**, 1697 (1977).
[28] H. Reiss, D. I. Margolese, and F. J. Shelling, J. Colloid Interface Sci. **56**, 511 (1976).
[29] P. Wegener and B. J. Wu, Faraday Discuss. Chem. Soc. **61**, 77 (1976).
[30] R. Strey and Y. Viisanen, J. Chem. Phys. **99**, 4693 (1993).
[31] J. L. Schmitt, J. Whitten, G. W. Adams, and R. A. Zalabsky, J. Chem. Phys. **92**, 3693 (1990).
[32] Y. Viisanen, R. Strey, A. Laaksonen, and M. Kulmala, J. Chem. Phys. **100**, 6062 (1994).
[33] R. Strey, Y. Viisanen, and P. E. Wagner, J. Chem. Phys. **103**, 4333 (1995).
[34] Y. Viisanen, P. E. Wagner, and R. Strey, J. Chem. Phys. **108**, 4257 (1998).
[35] M. Frish, R. Waterhouse, and G. Wilemski, Proceedings of the Fifth Symposium of Energy Engineering Sciences, Argonne, IL, June 1987, p. 115.
[36] B. J. C. Wu, P. P. Wegener, and G. D. Stein, J. Chem. Phys. **68**, 308 (1978).
[37] D. W. Oxtoby and D. Kashchiev, J. Chem. Phys. **100**, 7665 (1994).
[38] A. Laaksonen and M. Kulmala, J. Chem. Phys. **95**, 6745 (1991).
[39] G. D. Stein, Ph.D. thesis, Yale University, New Haven, CT, 1967.
[40] J. B. Young, PhysicoChem. Hydrodynam. **3**, 57 (1982).
[41] P. G. Hill, J. Fluid Mech. **25**, 593 (1966).
[42] *Lange's Handbook of Chemistry*, 14th ed., edited by J. A. Dean (McGraw–Hill, New York, 1992).
[43] The correlation is due to W. Wagner, ''A new correlation method for thermodynamic data applied to the vapor-pressure curve of argon, nitrogen and water,'' Report PC/T 15, IUPAC Thermodynamic Tables Project Centre, Dept. of Chemical Engineering and Chemical Technology, London, England. (1977); translation of doctoral disertation Forschr.-Ber VDI-Z/ Reihe 3, NR, 39, 1974 (in German); It is also presented in P. G. Hill and R. D. C. MacMillan, Ind. Eng. Chem. Fundam. **18**, 412 (1979).
[44] A. A. Pouring, Ph.D. thesis, Yale University, New Haven, CT, 1963.
[45] G. Wilemski and B. E. Wyslouzil, J. Chem. Phys. **103**, 1127 (1995).
[46] M. Tarek and M. Klein, J. Phys. Chem. **101**, 8639 (1997).
[47] G. Wilemski, in *Nucleation and Atmospheric Aerosols*, edited by N. Fukuta and P. E. Wagner (Deepak, Hampton, 1992) p. 71.